A Search for MeV to TeV Neutrinos from Fast Radio Bursts with IceCube

M. G. Aartsen[1], M. Ackermann[2], J. Adams[1], J. A. Aguilar[3], M. Ahlers[4], M. Ahrens[5], C. Alispach[6], K. Andeen[7], T. Anderson[8], I. Ansseau[3], G. Anton[9], C. Argüelles[10], J. Auffenberg[11], S. Axani[10], P. Backes[11], H. Bagherpour[1], X. Bai[12], A. Balagopal V.[13], A. Barbano[6], S. W. Barwick[14], B. Bastian[2], V. Baum[15], S. Baur[3], R. Bay[16], J. J. Beatty[17,18], K.-H. Becker[19], J. Becker Tjus[20], S. BenZvi[21], D. Berley[22], E. Bernardini[2,55], D. Z. Besson[23,56], G. Binder[16,24], D. Bindig[19], E. Blaufuss[22], S. Blot[2], C. Bohm[5], M. Börner[25], S. Böser[15], O. Botner[26], J. Böttcher[11], E. Bourbeau[4], J. Bourbeau[27], F. Bradascio[2], J. Braun[27], S. Bron[6], J. Brostean-Kaiser[2], A. Burgman[26], J. Buscher[11], R. S. Busse[28], T. Carver[6], C. Chen[29], E. Cheung[22], D. Chirkin[27], S. Choi[30], K. Clark[31], L. Classen[28], A. Coleman[32], G. H. Collin[10], J. M. Conrad[10], P. Coppin[33], P. Correa[33], D. F. Cowen[8,34], R. Cross[21], P. Dave[29], C. De Clercq[33], J. J. DeLaunay[8], H. Dembinski[32], K. Deoskar[5], S. De Ridder[35], P. Desiati[27], K. D. de Vries[33], G. de Wasseige[33], M. de With[36], T. DeYoung[37], A. Diaz[10], J. C. Díaz-Vélez[27], H. Dujmovic[30], M. Dunkman[8], E. Dvorak[12], B. Eberhardt[27], T. Ehrhardt[15], P. Eller[8], R. Engel[13], P. A. Evenson[32], S. Fahey[27], A. R. Fazely[38], J. Felde[22], K. Filimonov[16], C. Finley[5], A. Franckowiak[2], E. Friedman[22], A. Fritz[15], T. K. Gaisser[32], J. Gallagher[39], E. Ganster[11], S. Garrappa[2], L. Gerhardt[24], K. Ghorbani[27], T. Glauch[40], T. Glüsenkamp[9], A. Goldschmidt[24], J. G. Gonzalez[32], D. Grant[37], Z. Griffith[27], S. Griswold[21], M. Günder[11], M. Gündüz[20], C. Haack[11], A. Hallgren[26], L. Halve[11], F. Halzen[27], K. Hanson[27], A. Haungs[13], D. Hebecker[36], D. Heereman[3], P. Heix[11], K. Helbing[19], R. Hellauer[22], F. Henningsen[40], S. Hickford[19], J. Hignight[41], G. C. Hill[42], K. D. Hoffman[22], R. Hoffmann[19], T. Hoinka[25], B. Hokanson-Fasig[27], K. Hoshina[27,57], F. Huang[8], M. Huber[40], T. Huber[2,13], K. Hultqvist[5], M. Hünnefeld[25], R. Hussain[27], S. In[30], N. Iovine[3], A. Ishihara[43], G. S. Japaridze[44], M. Jeong[30], K. Jero[27], B. J. P. Jones[45], F. Jonske[11], R. Joppe[11], D. Kang[13], W. Kang[30], A. Kappes[28], D. Kappesser[15], T. Karg[2], M. Karl[40], A. Karle[27], U. Katz[9], M. Kauer[27], J. L. Kelley[27], A. Kheirandish[27], J. Kim[30], T. Kintscher[2], J. Kiryluk[46], T. Kittler[9], S. R. Klein[16,24], R. Koirala[32], H. Kolanoski[36], L. Köpke[15], C. Kopper[37], S. Kopper[47], D. J. Koskinen[4], M. Kowalski[2,36], K. Krings[40], G. Krückl[15], N. Kulacz[41], N. Kurahashi[48], A. Kyriacou[42], M. Labare[35], J. L. Lanfranchi[8], M. J. Larson[22], F. Lauber[19], J. P. Lazar[27], K. Leonard[27], A. Leszczyńska[13], M. Leuermann[11], Q. R. Liu[27], E. Lohfink[15], C. J. Lozano Mariscal[28], L. Lu[43], F. Lucarelli[6], J. Lünemann[33], W. Luszczak[27], Y. Lyu[16,24], W. Y. Ma[2], J. Madsen[49], G. Maggi[33], K. B. M. Mahn[37], Y. Makino[43], P. Mallik[11], K. Mallot[27], S. Mancina[27], I. C. Mariş[3], R. Maruyama[50], K. Mase[43], R. Maunu[22], F. McNally[51], K. Meagher[27], M. Medici[4], A. Medina[18], M. Meier[25], S. Meighen-Berger[40], T. Menne[25], G. Merino[27], T. Meures[3], J. Micallef[37], D. Mockler[3], G. Momenté[15], T. Montaruli[6], R. W. Moore[41], R. Morse[27], M. Moulai[10], P. Muth[11], R. Nagai[43], U. Naumann[19], G. Neer[37], H. Niederhausen[40], S. C. Nowicki[37], D. R. Nygren[24], A. Obertacke Pollmann[19], M. Oehler[13], A. Olivas[22], A. O'Murchadha[3], E. O'Sullivan[5], T. Palczewski[16,24], H. Pandya[32], D. V. Pankova[8], N. Park[27], P. Peiffer[15], C. Pérez de los Heros[26], S. Philippen[11], D. Pieloth[25], E. Pinat[3], A. Pizzuto[27], M. Plum[7], A. Porcelli[35], P. B. Price[16], G. T. Przybylski[24], C. Raab[3], A. Raissi[1], M. Rameez[4], L. Rauch[2], K. Rawlins[52], I. C. Rea[40], R. Reimann[11], B. Relethford[48], M. Renschler[13], G. Renzi[3], E. Resconi[40], W. Rhode[25], M. Richman[48], S. Robertson[24], M. Rongen[11], C. Rott[30], T. Ruhe[25], D. Ryckbosch[35], D. Rysewyk[37], I. Safa[27], S. E. Sanchez Herrera[37], A. Sandrock[25], J. Sandroos[15], M. Santander[47], S. Sarkar[53], S. Sarkar[41], K. Satalecka[2], M. Schaufel[11], H. Schieler[13], P. Schlunder[25], T. Schmidt[22], A. Schneider[27], J. Schneider[9], F. G. Schröder[13,32], L. Schumacher[11], S. Sclafani[48], D. Seckel[32], S. Seunarine[49], S. Shefali[11], M. Silva[27], R. Snihur[27], J. Soedingrekso[25], D. Soldin[32], M. Song[22], G. M. Spiczak[49], C. Spiering[2], J. Stachurska[2], M. Stamatikos[18], T. Stanev[32], R. Stein[2], P. Steinmüller[13], J. Stettner[11], A. Steuer[15], T. Stezelberger[24], R. G. Stokstad[24], A. Stößl[43], N. L. Strotjohann[2], T. Stürwald[11], T. Stuttard[4], G. W. Sullivan[22], I. Taboada[29], F. Tenholt[20], S. Ter-Antonyan[38], A. Terliuk[2], S. Tilav[32], K. Tollefson[37], L. Tomankova[20], C. Tönnis[30], S. Toscano[3], D. Tosi[27], A. Trettin[2], M. Tselengidou[9], C. F. Tung[29], A. Turcati[40], R. Turcotte[13], C. F. Turley[8], B. Ty[27], E. Unger[26], M. A. Unland Elorrieta[28], M. Usner[2], J. Vandenbroucke[27], W. Van Driessche[35], D. van Eijk[27], N. van Eijndhoven[33], S. Vanheule[35], J. van Santen[2], M. Vraeghe[35], C. Walck[5], A. Wallace[42], M. Wallraff[11], N. Wandkowsky[27], T. B. Watson[45], C. Weaver[41], A. Weindl[13], M. J. Weiss[8], J. Weldert[15], C. Wendt[27], J. Werthebach[27], B. J. Whelan[42], N. Whitehorn[54], K. Wiebe[15], C. H. Wiebusch[11], L. Wille[27], D. R. Williams[47], L. Wills[48], M. Wolf[40], J. Wood[27], T. R. Wood[41], K. Woschnagg[16], G. Wrede[9], D. L. Xu[27], X. W. Xu[38], Y. Xu[46], J. P. Yanez[41], G. Yodh[14], S. Yoshida[43], T. Yuan[27], and M. Zöcklein[11]

IceCube Collaboration

[1] Department of Physics and Astronomy, University of Canterbury, Private Bag 4800, Christchurch, New Zealand; analysis@icecube.wisc.edu
[2] DESY, D-15738 Zeuthen, Germany
[3] Université Libre de Bruxelles, Science Faculty CP230, B-1050 Brussels, Belgium
[4] Niels Bohr Institute, University of Copenhagen, DK-2100 Copenhagen, Denmark
[5] Oskar Klein Centre and Department of Physics, Stockholm University, SE-10691 Stockholm, Sweden
[6] Département de Physique Nucléaire et Corpusculaire, Université de Genève, CH-1211 Genève, Switzerland
[7] Department of Physics, Marquette University, Milwaukee, WI, 53201, USA
[8] Department of Physics, Pennsylvania State University, University Park, PA 16802, USA
[9] Erlangen Centre for Astroparticle Physics, Friedrich-Alexander-Universität Erlangen-Nürnberg, D-91058 Erlangen, Germany
[10] Department of Physics, Massachusetts Institute of Technology, Cambridge, MA 02139, USA
[11] III. Physikalisches Institut, RWTH Aachen University, D-52056 Aachen, Germany
[12] Physics Department, South Dakota School of Mines and Technology, Rapid City, SD 57701, USA
[13] Karlsruhe Institute of Technology, Institut für Kernphysik, D-76021 Karlsruhe, Germany
[14] Department of Physics and Astronomy, University of California, Irvine, CA 92697, USA

[15] Institute of Physics, University of Mainz, Staudinger Weg 7, D-55099 Mainz, Germany
[16] Department of Physics, University of California, Berkeley, CA 94720, USA
[17] Department of Astronomy, Ohio State University, Columbus, OH 43210, USA
[18] Department of Physics and Center for Cosmology and Astro-Particle Physics, Ohio State University, Columbus, OH 43210, USA
[19] Department of Physics, University of Wuppertal, D-42119 Wuppertal, Germany
[20] Fakultät für Physik & Astronomie, Ruhr-Universität Bochum, D-44780 Bochum, Germany
[21] Department of Physics and Astronomy, University of Rochester, Rochester, NY 14627, USA
[22] Department of Physics, University of Maryland, College Park, MD 20742, USA
[23] Department of Physics and Astronomy, University of Kansas, Lawrence, KS 66045, USA
[24] Lawrence Berkeley National Laboratory, Berkeley, CA 94720, USA
[25] Department of Physics, TU Dortmund University, D-44221 Dortmund, Germany
[26] Department of Physics and Astronomy, Uppsala University, Box 516, SE-75120 Uppsala, Sweden
[27] Department of Physics and Wisconsin IceCube Particle Astrophysics Center, University of Wisconsin, Madison, WI 53706, USA
[28] Institut für Kernphysik, Westfälische Wilhelms-Universität Münster, D-48149 Münster, Germany
[29] School of Physics and Center for Relativistic Astrophysics, Georgia Institute of Technology, Atlanta, GA 30332, USA
[30] Department of Physics, Sungkyunkwan University, Suwon 16419, Republic of Korea
[31] SNOLAB, 1039 Regional Road 24, Creighton Mine 9, Lively, ON, P3Y 1N2, Canada
[32] Bartol Research Institute and Department of Physics and Astronomy, University of Delaware, Newark, DE 19716, USA
[33] Vrije Universiteit Brussel (VUB), Dienst ELEM, B-1050 Brussels, Belgium
[34] Department of Astronomy and Astrophysics, Pennsylvania State University, University Park, PA 16802, USA
[35] Department of Physics and Astronomy, University of Gent, B-9000 Gent, Belgium
[36] Institut für Physik, Humboldt-Universität zu Berlin, D-12489 Berlin, Germany
[37] Department of Physics and Astronomy, Michigan State University, East Lansing, MI 48824, USA
[38] Department of Physics, Southern University, Baton Rouge, LA 70813, USA
[39] Department of Astronomy, University of Wisconsin, Madison, WI 53706, USA
[40] Physik-department, Technische Universität München, D-85748 Garching, Germany
[41] Department of Physics, University of Alberta, Edmonton, Alberta, T6G 2E1, Canada
[42] Department of Physics, University of Adelaide, Adelaide, 5005, Australia
[43] Department of Physics and Institute for Global Prominent Research, Chiba University, Chiba 263-8522, Japan
[44] CTSPS, Clark-Atlanta University, Atlanta, GA 30314, USA
[45] Department of Physics, University of Texas at Arlington, 502 Yates Street, Science Hall Room 108, Box 19059, Arlington, TX 76019, USA
[46] Department of Physics and Astronomy, Stony Brook University, Stony Brook, NY 11794-3800, USA
[47] Department of Physics and Astronomy, University of Alabama, Tuscaloosa, AL 35487, USA
[48] Department of Physics, Drexel University, 3141 Chestnut Street, Philadelphia, PA 19104, USA
[49] Department of Physics, University of Wisconsin, River Falls, WI 54022, USA
[50] Department of Physics, Yale University, New Haven, CT 06520, USA
[51] Department of Physics, Mercer University, Macon, GA 31207-0001, Georgia
[52] Department of Physics and Astronomy, University of Alaska Anchorage, 3211 Providence Drive, Anchorage, AK 99508, USA
[53] Department of Physics, University of Oxford, Parks Road, Oxford OX1 3PU, UK
[54] Department of Physics and Astronomy, UCLA, Los Angeles, CA 90095, USA

Abstract

We present two searches for IceCube neutrino events coincident with 28 fast radio bursts (FRBs) and 1 repeating FRB. The first improves on a previous IceCube analysis—searching for spatial and temporal correlation of events with FRBs at energies greater than roughly 50 GeV—by increasing the effective area by an order of magnitude. The second is a search for temporal correlation of MeV neutrino events with FRBs. No significant correlation is found in either search; therefore, we set upper limits on the time-integrated neutrino flux emitted by FRBs for a range of emission timescales less than one day. These are the first limits on FRB neutrino emission at the MeV scale, and the limits set at higher energies are an order-of-magnitude improvement over those set by any neutrino telescope.

1. Introduction

The IceCube Neutrino Observatory instruments $1 \, \text{km}^3$ of Antarctic ice between depths of 1450 and 2450 m at the geographic South Pole and records particle interactions in the ice by capturing Cerenkov radiation, produced by secondary particles, in photomultiplier tubes that are housed in a glass pressure vessel known as digital optical modules (DOMs; Aartsen et al. 2017). IceCube observes a cosmic neutrino flux from 10 TeV to a few PeV (Aartsen et al. 2015a, 2015b) and

recently reported evidence for neutrino emission from the blazar TXS 0506+056 (Aartsen et al. 2018b, 2018c).

Despite the evidence for neutrino emission from TXS 0506+056, the overwhelming majority of the diffuse astrophysical flux remains unexplained. Transient sources play a major role in high-energy astrophysics and potentially could account for a large fraction of the detected neutrino flux. Fast radio bursts (FRBs) are a class of nonperiodic, highly dispersed, millisecond-scale radio flashes (Keane 2018; Lorimer 2018). Although fewer than 60 unique sources have been detected, the expected rate of detectable FRBs each day is in the thousands (Bhandari et al. 2018). Many models for FRBs have been offered (Platts et al. 2018), but due to the scarcity of discoveries and multiwavelength follow-up detections, none is strongly favored. Some of these models allow for hadronic
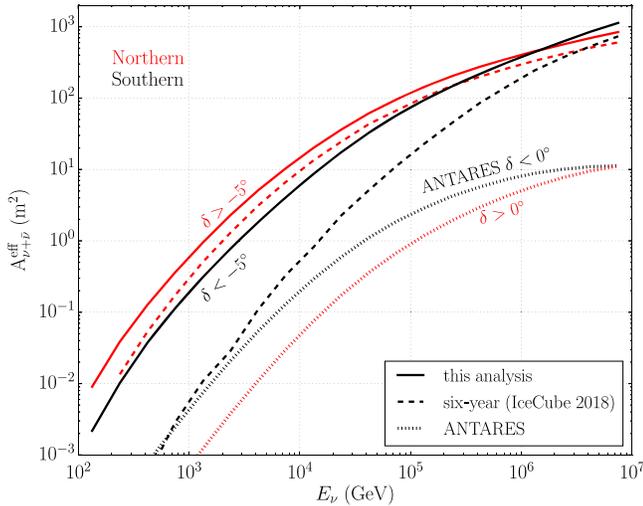
Figure 1. With an event selection looser than that in IceCube's six years analysis searching for neutrinos from FRBs (Aartsen et al. 2018a), the effective area of this selection to muon neutrinos is improved significantly, especially in the southern sky (black) and at energies less than 1 PeV. This is compared to the smaller effective area of ANTARES for a point-source event selection (Albert et al. 2017) that approximately reproduces the effective area from their 2018 FRB analysis (see Figure 5 in Albert et al. 2019).

acceleration in the vicinity of the progenitors, such as super massive neutron stars, or supernova explosions, which would lead to the production of both high-energy cosmic rays and neutrinos (Li et al. 2014; Das Gupta & Saini 2017).

Previous analyses have set upper limits on neutrino emission from FRBs, using quality tracklike events in IceCube (Fahey et al. 2017; Aartsen et al. 2018a). A search for multiplets of tracklike neutrino events with minute-scale temporal coincidence limits the number density of a transient source class, under particular source evolution assumption, producing IceCube astrophysical flux to larger than 10^{-5} Mpc^{-3} yr^{-1} (Aartsen et al. 2019); the numerous and dim emission from FRBs is consistent with this lower bound (Callister et al. 2016).

This work includes two analyses that improve existing constraints on neutrino emission from FRBs and test a wider range of neutrino energies. IceCube has access to two different energy ranges, and we take advantage of that to search for coincidences with FRBs. In Section 2, we present a search using a tracklike event selection with improved effective area compared to previous IceCube searches. In Section 3, we present a search for temporal correlation of MeV neutrinos with FRBs. Section 4 summarizes analysis results and discusses the outlook for future searches for neutrinos from FRBs.

2. Search for Coincident Muon Track Events

This search uses a procedure similar to that of IceCube's previous search for neutrino emission from FRBs (Aartsen et al. 2018a), which is hereafter referred to as the six years analysis. These analyses search for both temporal and spatial correlation of FRBs and muon neutrino events, in which a muon created from a charged-current interaction leaves a tracklike signature in the detector. All 28 nonrepeating FRBs are analyzed (Table 1) in a source-stacking search and in a search for the brightest source. The six years analysis used an event selection that was initially optimized for analyses of

Table 1
SNDAQ Search Results for the Most Significant Bursts in the Analysis

FRB	ΔT (ms)	Significance (Before Muon Correction)	Significance (After Muon Correction)
121102 b1	640	2.97	0.88
121102 b1	1280	3.03	0.85
131104	1280	3.57	2.55

gamma-ray bursts. Because FRBs have much shorter durations, higher levels of background are tolerated, and we can use a looser event selection procedure to increase acceptance to astrophysical muon neutrinos and improve analysis sensitivity at emission timescales less than 10^3 s.

2.1. Event Sample

The data used in this analysis consist of through-going muon neutrino candidate events from 2011 February 18 through 2018 March 13. In the six years analysis, to reduce the fraction of atmospheric muons in the sample, the data consisted largely of events with very high energy ($E_\nu > 10$ TeV) or events that had penetrated many kilometers of ice prior to detection. Here, we instead use an event selection closer to IceCube's trigger level, resulting in a higher rate of atmospheric muons but increasing the acceptance of astrophysical neutrinos as well. This event selection focuses on removing low-energy events so that passing data can be transmitted via satellite within the bandwidth limit of roughly 75 gigabytes per day.

The sample of muon track events has an average all-sky rate of 35.7 Hz, due mainly to penetrating muons from cosmic-ray interactions in Earth's atmosphere. Roughly five events per day are caused by astrophysical muon neutrinos.[58] Compared to the six years analysis, the effective area of this event selection to muon neutrinos is an order of magnitude larger in the southern sky (Figure 1), with the largest improvements coming from energies less than 100 TeV. In the northern sky, where the Earth already attenuates the atmospheric muon background, the average improvement is roughly 50% in effective area. Correspondingly, the background rate for this event selection is much larger than that for the six years analysis. Figure 2 compares the distribution of background data versus the zenith angle for the six years analysis to this event selection; the peak-to-peak seasonal variation in this rate is about 25%, with a maximum rate occurring in January, the austral summer.[59]

A total of 28 nonrepeating FRBs were analyzed in this search. Information about each FRB is presented in Table 2.

2.2. Analysis Method

The test statistic (TS) defined here is similar to that of the six years analysis (Aartsen et al. 2018a). For a search time window ΔT, temporal correlation of an event with an FRB is satisfied if the event triggers the detector in the interval $[t_{\mathrm{FRB}} - \Delta T/2, \ t_{\mathrm{FRB}} + \Delta T/2]$. Using a model-independent

---

[58] This estimate is calculated by combining the effective area of the event selection with IceCube's global fit of the diffuse astrophysical neutrino flux (Aartsen et al. 2015a), which is an $E^{-2.49}$ unbroken power law.

[59] Seasonal variation in atmospheric density affects the fraction of cosmic-ray-produced pions and kaons that decay, producing ice-penetrating muons, before otherwise interacting in the air. This causes IceCube's trigger rate, due to atmospheric muons, to peak in the austral summer. For more details on seasonal variation, see Grashorn et al. (2010), Tilav et al. (2010), Desiati (2011), and references therein.

Table 2
Analysis of 39 FRBs from 29 Unique Directions

FRB	SNDAQ	Tracks	Time (UTC)	Duration (ms)	R.A.	Decl.
FRB 110220	✓	✓	2011 Feb 20 01:55:48.957	5.6	22h 34′	−12° 24′
FRB 110523	✓	✓	2011 May 23 15:06:19.738	1.73	21^h 45′	−00° 12′
FRB 110626	✓	✓	2011 Jun 26 21:33:17.474	<1.4	21^h 03′	−44° 44′
FRB 110703	⋯	✓	2011 Jul 3 18:59:40.591	<4.3	23^h 30′	−02° 52′
FRB 120127	✓	✓	2012 Jan 27 08:11:21.723	<1.1	23^h 15′	−18° 25′
FRB 121002	✓	✓	2012 Oct 2 13:09:18.402	2.1; 3.7	18^h 14′	−85° 11′
FRB 121102 b0	✓	⋯	2012 Nov 2 06:47:17.117	3.3	05^h 32′	+33° 05′
FRB 130626	✓	✓	2013 Jun 26 14:56:00.06	<0.12	16^h 27′	−07° 27′
FRB 130628	✓	✓	2013 Jun 28 03:58:00.02	<0.05	09^h 03′	+03° 26′
FRB 130729	✓	✓	2013 Jul 29 09:01:52.64	<4	13^h 41′	−05° 59′
FRB 131104	✓	✓	2013 Nov 4 18:04:01.2	<0.64	06^h 44′	−51° 17′
FRB 140514	⋯	✓	2014 May 14 17:14:11.06	2.8	22^h 34′	−12° 18′
FRB 150215	⋯	✓	2015 Feb 15 20:41:41.714	2.88	18^h 17′	−4° 54′
FRB 150418	✓	✓	2015 Apr 18 04:29:05.370	0.8	07^h 16′	−19° 00′
FRB 121102 b1	✓	⋯	2015 May 17 17:42:08.712	3.8	05^h 32′	+33° 05′
FRB 121102 b2	✓	⋯	2015 May 17 17:51:40.921	3.3	05^h 32′	+33° 05′
FRB 121102 b3	✓	⋯	2015 Jun 2 16:38:07.575	4.6	05^h 32′	+33° 05′
FRB 121102 b4	✓	⋯	2015 Jun 2 16:47:36.484	8.7	05^h 32′	+33° 05′
FRB 121102 b5	✓	⋯	2015 Jun 2 17:49:18.627	2.8	05^h 32′	+33° 05′
FRB 121102 b6	✓	⋯	2015 Jun 2 17:49:41.319	6.1	05^h 32′	+33° 05′
FRB 121102 b7	✓	⋯	2015 Jun 2 17:50:39.298	6.6	05^h 32′	+33° 05′
FRB 121102 b8	✓	⋯	2015 Jun 2 17:53:45.528	6.0	05^h 32′	+33° 05′
FRB 121102 b9	✓	⋯	2015 Jun 2 17:56:34.787	8.0	05^h 32′	+33° 05′
FRB 121102 b10	✓	⋯	2015 Jun 2 17:57:32.020	3.1	05^h 32′	+33° 05′
FRB 150610	⋯	✓	2015 Jun 10 05:26:59.396	2.00	10^h 44′	−40° 05′
FRB 150807	⋯	✓	2015 Aug 7 17:53:55.83	0.35	22^h 43′	−55° 05′
FRB 151206	⋯	✓	2015 Dec 6 06:17:52.778	3.00	19^h 21′	−04° 08′
FRB 151230	⋯	✓	2015 Dec 30 16:15:46.525	4.40	09^h 40′	−03° 27′
FRB 160102	⋯	✓	2016 Jan 2 08:28:39.374	3.40	22^h 39′	−30° 11′
FRB 160317	⋯	✓	2016 Mar 17 09:00:36.53	21.00	07^h 54′	−29° 37′
FRB 160410	⋯	✓	2016 Apr 10 08:33:39.68	4.00	08^h 41′	+06° 05′
FRB 160608	⋯	✓	2016 Jun 8 03:53:01.088	9.00	07^h 37′	−40° 48′
FRB 170107	⋯	✓	2017 Jan 7 20:05:45.139	2.60	11^h 23′	−05° 00′
FRB 170827	⋯	✓	2017 Aug 27 16:20:18	0.40	00^h 49′	−65° 33′
FRB 170922	⋯	✓	2017 Sep 22 11:22:23.40	26.00	21^h 30′	−08° 00′
FRB 171209	⋯	✓	2017 Dec 9 20:34:23.50	2.50	15^h 50′	−46° 10′
FRB 180301	⋯	✓	2018 Mar 1 07:34:19.76	3.00	06^h 13′	+04° 34′
FRB 180309	⋯	✓	2018 Mar 9 02:49:32.99	0.58	21^h 25′	−33° 59′
FRB 180311	⋯	✓	2018 Mar 11 04:11:54.80	12.00	21^h 32′	−57° 44′

Note. Checkmarks (✓) indicate that an FRB is analyzed in the MeV (SNDAQ) and/or GeV–TeV (Tracks) stream. The latter included all nonrepeating FRBs. Repeated bursts from FRB 121102 are labeled with an additional "b0," "b1," and so on. Additional burst characteristics were taken from www.frbcat.org (Petroff et al. 2016): arrival time and duration corrected for signal dispersion, R.A., and decl. (J2000) are rounded to the nearest arcminute.

maximum likelihood method, events temporally coincident with a single FRB contribute to the maximum likelihood ratio TS, defined as

$$\mathrm{TS} = -\hat{n}_s + \sum_{i=1}^{N} \ln\left[1 + \frac{\hat{n}_s S(x_i)}{n_b B(x_i)}\right], \qquad (1)$$

where $S(x_i)$ is the total spatial probability density distribution that considers the angular distance of an event direction x_i with respect to the coordinates of a given FRB and where $B(x_i)$ combines separate spatial and temporal parameterizations of data to describe the background probability density distribution in that time and direction. Here, n_b is the expected number of background events in ΔT, and likelihood is maximized with respect to the best-fit number of observed signal events, $\hat{n}_s$. In the stacking search, the TS in Equation (1) will have an additional sum over the number of FRBs in the search.

As in the six years analysis, two tests are performed. The stacking test, which tests the hypothesis that the astrophysical class of FRBs emits neutrinos, evaluates the TS for all events in ΔT centered on all sources. The max-burst test, which tests the hypothesis that among a heterogeneous class of FRBs, one or a few bright sources emit neutrinos, evaluates a TS separately for each FRB and its respective events, returning only the largest TS as the observation at ΔT. In the stacking test, we consider a range of neutrino emission timescales by evaluating expanding iterations of ΔT from 0.03 10^5 s: $\Delta T = 0.01 \cdot 10^{i/2}$ s, where $i = 1, 2, \ldots,$ 14. Beyond $\Delta T > 10^3$ s, the sensitivity of the max-burst analysis exceeds upper limits set in the six years analysis for all tested spectra; therefore, we do not evaluate larger ΔT for the max-burst test.

2.3. Results

We find the results from both the stacking test and the max-burst test consistent with the background-only hypothesis
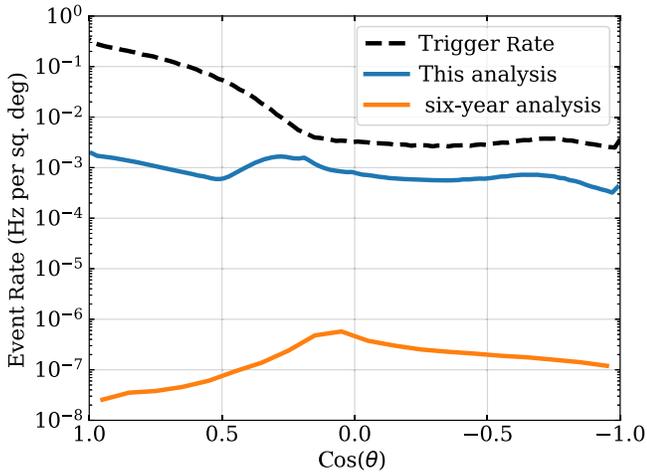
Figure 2. The event rate for these data is about $4000\times$ larger than that for the six years analysis data, for almost all zenith angles, θ, due mostly to an increase in the number of muons generated by cosmic rays passing the event selection. The increase is largest in the southern sky ($\cos(\theta) > 0$), approaching a factor of 10^5 increase at zenith. Features in the southern sky are the result of selection methods (e.g., the deposited energy required to pass event selection is higher for events with $\theta < 70°$).

Table 3
TS Values for Stacking and Max-burst Tests in Each ΔT of the High-energy (Muon Tracks) Search

ΔT (s)	Stacking TS Median	Result	p	Max-source TS Median	Result	p
3.16e−2	0	0	1	1.13	0.32	0.87
1.00e−1	0	0	1	1.21	1.10	0.54
3.16e−1	0	0	1	1.30	1.31	0.49
1.00e−0	0	0	1	1.40	0.12	0.98
3.16e−0	0	0	1	1.54	1.35	0.57
1.00e+1	0	0.29	0.124	1.76	2.38	0.32
3.16e+1	0	0.02	0.256	2.03	2.85	0.27
1.00e+2	0	0.07	0.274	2.44	4.86	0.07
3.16e+2	0	0	1	3.22	6.06	0.08
1.00e+3	0.024	2.32	0.042	5.05	10.57	0.05
3.16e+3	0.208	1.64	0.141	⋯	⋯	⋯
1.00e+4	0.779	0.79	0.492	⋯	⋯	⋯
3.16e+4	2.559	0	1	⋯	⋯	⋯
1.00e+5	8.023	0	1	⋯	⋯	⋯

Note. The median TS values from 10^9 trials of background-only simulation are shown for comparison, along with pretrial p-values for results in their respective ΔT. For the max-burst analysis, we test only the ΔTs for which there is an improvement in sensitivity relative to the six years analysis. Both tests produce most significant results in $\Delta T = 10^3$ s; posttrial significance for the stacking and max-source tests is $p = 0.35$ and $p = 0.33$, respectively.

(Table 3). After trials correcting each test for the number of time windows searched,[60] the p-values for the stacking and max-burst tests are 0.35 and 0.33, respectively.

Upper limits are calculated (90% confidence level) for the time-integrated flux per FRB at each ΔT (Figure 3). The results

---

[60] Test results from consecutive time windows are correlated in this analysis, as the smaller time windows are contained within the larger time windows. Therefore, the trials factor is less than the number of windows searched. A Monte Carlo simulation calculates the probability of exceeding the smallest pretrial p-value over the course of expansion of ΔT, and this probability is known as the posttrial p-value.

Table 4
Upper Limits (90% C.L.) on the Time-integrated E^{-2} Power-law Flux from 28 FRBs

FRB	IceCube U.L.	ANTARES U.L.
FRB 110220	0.0258	⋯
FRB 110523	0.0206	⋯
FRB 110626	0.112	⋯
FRB 110703	0.0204	⋯
FRB 120127	0.0353	⋯
FRB 121002	0.175	⋯
FRB 130626	0.0222	⋯
FRB 130628	0.0208	⋯
FRB 130729	0.0208	⋯
FRB 131104	0.129	1.1
FRB 140514	0.0262	1.9
FRB 150215	0.0204	2.3
FRB 150418	0.0390	1.7
FRB 150610	0.105	⋯
FRB 150807	0.134	1.6
FRB 151206	0.0212	1.3
FRB 151230	0.0203	1.6
FRB 160102	0.0755	2.0
FRB 160317	0.0689	1.6
FRB 160410	0.0213	1.5
FRB 160608	0.0995	2.1
FRB 170107	0.0213	1.1
FRB 170827	0.147	⋯
FRB 170922	0.0214	⋯
FRB 171209	0.124	⋯
FRB 180301	0.0210	⋯
FRB 180309	0.0832	⋯
FRB 180311	0.139	⋯

Note. This high-energy analysis sets upper limits on FRB neutrino emission on timescales similar to the radio emission ($\Delta T = 30$ms), and we compare these to limits set by ANTARES with $\Delta T = 12$ hr for 12 FRBs (Abbasi et al. 2017).

are listed in Table 4. In the stacking search (top panels), the limits we set for $\Delta T < 1$ s are factors of 10 and 50 stronger on spectra of E^{-2} and E^{-3}, respectively. We compare to the southern sky results of the six years analysis because that search also excluded the repeater and tested the majority of single-burst FRBs available at the time. In the max-burst search (bottom panels), the same scale of improvement is made on the maximum flux among 28 sources at the smallest ΔT.

3. Search for Coincident MeV Neutrino Data

IceCube is primarily designed to detect neutrinos with energies greater than 100 GeV, targeting sources with TeV neutrino emission. However, IceCube can measure a large burst of MeV neutrinos by detecting a collective rise in all photomultiplier rates on the top of the background noise. Although the increase in the counting rate in each light sensor is not statistically significant, the effect will be clearly seen once the rise is considered collectively over many sensors. This technique was originally developed for searches for $\mathcal{O}(10\,\mathrm{MeV})$ neutrinos from supernovae. IceCube utilizes a real-time data stream called the Supernova Data Acquisition (SNDAQ) system to identify collective rises in the rates of photomultipliers across the detector (Abbasi et al. 2011). We use the SNDAQ data stream to search for MeV neutrinos from FRBs.

The signals from photomultiplier tubes, also called DOM hits, are counted in 2 ms bins by SNDAQ. Here, we use this
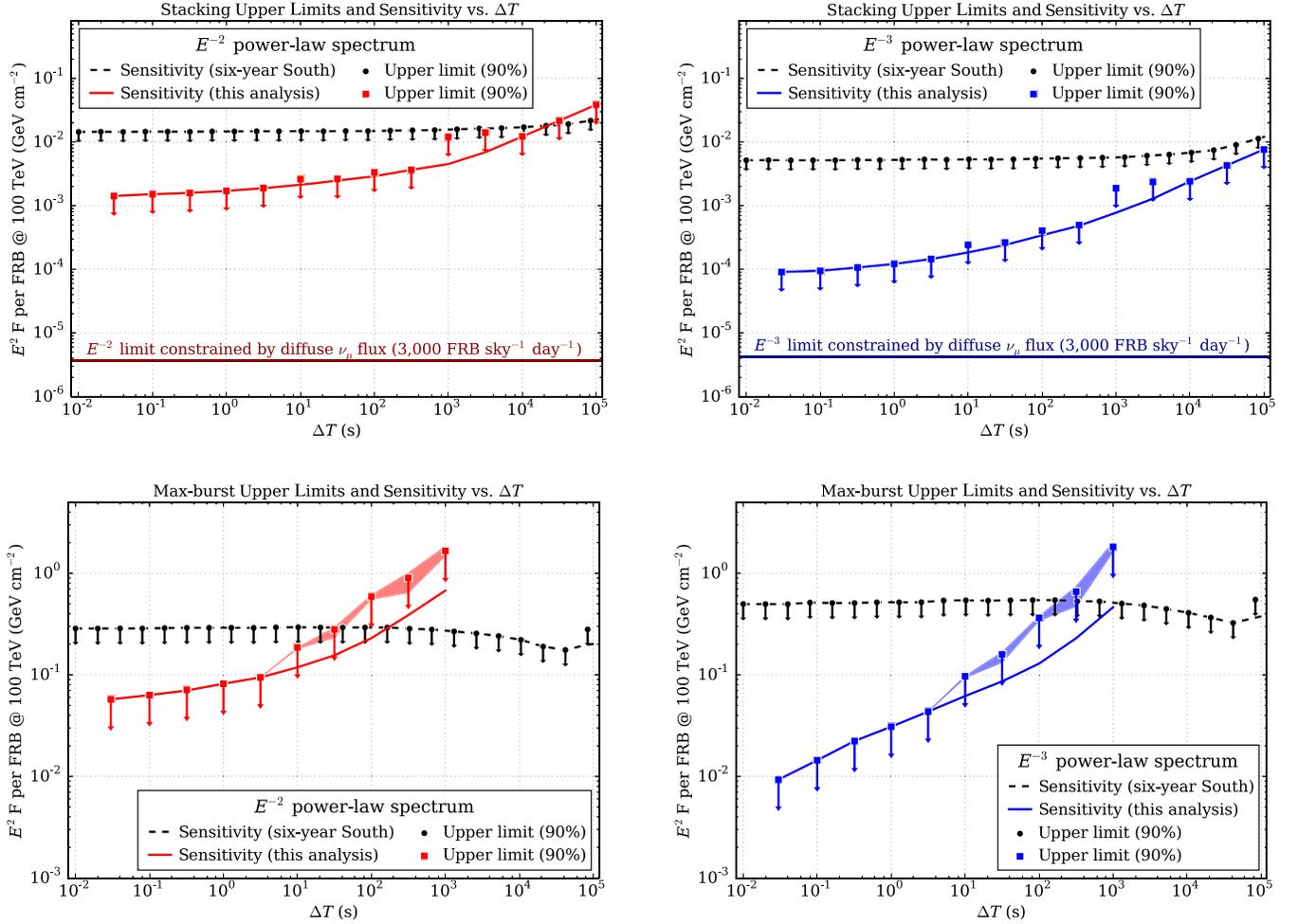
Figure 3. We set upper limits on the time-integrated neutrino flux per FRB for a range of ΔT, assuming power-law spectra of E^{-2} (top left) and E^{-3} (top right). These limits provide an order-of-magnitude improvement over the previous best limits on nonrepeating FRBs (Aartsen et al. 2018a). For comparison, we show constraints produced by dividing IceCube's entire astrophysical ν_μ flux (Haack & Weibush 2017) equally among a homogeneous class of 3000 FRBs per day. We also set upper limits on the maximum time-integrated neutrino flux among 28 FRBs for every ΔT, assuming power-law spectra of E^{-2} (bottom left) and E^{-3} (bottom right). The error bands on these limits represent the central 90% of systematic variation in limits due to uncertainty in background parameterization.

data stream and search for neutrino signals from the 21 FRBs for which data were available. In this search, different bursts of the repeating FRB (FRB 121102) are considered as individual sources.

3.1. Analysis Method

To find an excess on top of the background noise rate in the detector, a one-dimensional Gaussian likelihood is used to determine the significance of a collective deviation ($\Delta\mu$) of the noise across the detector.

$$\mathcal{L}(\Delta\mu) = \prod_{i=1}^{N_{\text{DOM}}} \frac{1}{\sqrt{2\pi}\,\langle\sigma_i\rangle} \exp\left(-\frac{(n_i - (\mu_i + \epsilon_i\,\Delta\mu))^2}{2\langle\sigma_i\rangle^2}\right),$$
(2)

where n_i is the per DOM$_i$ rate in a chosen time bin, ϵ_i is a DOM-specific efficiency parameter that accounts for module- and depth-dependent detection probabilities, and μ_i and σ_i are the mean and standard deviation for individual DOMs. Maximizing the log-likelihood with respect to $\Delta\mu$, one finds

$$\Delta\mu = \sigma_{\Delta\mu}^2 \sum_{i=1}^{N_{\text{DOM}}} \frac{\epsilon_i(n_i - \mu_i)}{\langle\sigma_i\rangle^2},$$
(3)

where

$$\sigma_{\Delta\mu}^2 = \left(\sum_{i=1}^{N_{\text{DOM}}} \frac{\epsilon_i^2}{\langle\sigma_i\rangle^2}\right)^{-1}.$$
(4)

If there is an excess in the rate across the detector, its significance, ξ, will be given by

$$\xi = \frac{\Delta\mu}{\sigma_{\Delta\mu}}.$$
(5)

To search for an increase in hits during the FRB period, we bin the data collected in the SNDAQ stream into bins of 10 ms. We search in eight different time windows from the lowest 10 ms and extending by powers of 2 up to a time window of 1280 ms. To estimate the background, we use data from a 10,240 ms background-only time window using the 8-hour runs before and after the actual FRB trigger. The background window excludes the signal time window, and its size does not change as we expand the signal window.

The distribution of the significance over the course of a run in IceCube is almost a Gaussian. We use the distribution of the significances, obtained from off-time windows before and after the run that includes each FRB, to obtain a threshold beyond which the significance would not arise from a random
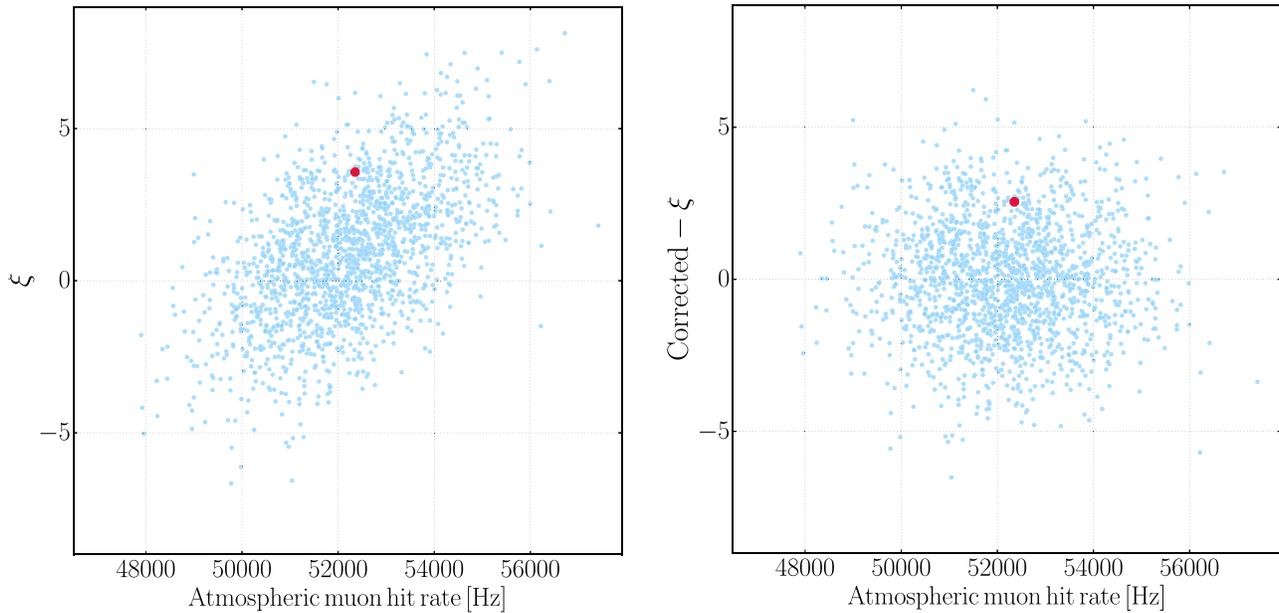
Figure 4. Correlation of significance (ξ) with atmospheric muon hit rates for the highest significance found in the sample (FRB 123202 with 1280 ms time window). The original significances (left) and corrected significances (right) are shown. The observed significance for the time of FRB is presented in red, and the off-time significances are in blue.

fluctuation of the background in the detector. We set a 3σ threshold (one-sided) in the significance to claim a discovery.

It has been shown that the rate of the hits in SNDAQ contains a contribution that is directly correlated with the seasonally changing rate of atmospheric muons traversing the detector. To remove this correlation, we subtract the muon dependency via linear regression as described in Baum et al. (2015). The 3σ threshold is reevaluated according to the corrected distribution. If the significance is found to be greater than the threshold set, we consider that a detection. Otherwise, we set upper limits for the absence of signal above the threshold.

3.2. Results

After obtaining the threshold for all time windows for the 21 FRBs considered in this analysis (see Table 2), we perform the likelihood analysis on the on-time window for each FRB.

No significance was found above the significance threshold in the data for the time FRBs happened. The three most significant searches are presented in Table 1. Figure 4 shows the observed significance before (left panel) and after (right panel) significance and the dependence of the significance on the atmospheric muon hit rates for the most significant FRB in the search. The distribution of the significances, along with the threshold and the observed significance for the most significant search, is shown in Figure 5. Given that no results were found beyond the threshold obtained from off-time periods, we set upper limits on the flux of antielectron neutrinos for each burst and time windows considered in this study.

The dependency of the signal hit rate on the flux of neutrinos is described in Abbasi et al. (2011). For the purpose of this analysis, in the absence of neutrino spectrum models for FRBs, we consider the neutrino emission from core collapse supernova as a fiducial model to obtain the upper limit on MeV neutrino emission. Here, the normalization was chosen such that it corresponds to a model describing the neutrino flux with average neutrino energy $E_\nu = 15.6$ MeV and pinching parameter $\alpha = 3$ (Totani et al. 1998), yielding $\langle E_{\nu 3}\rangle =$
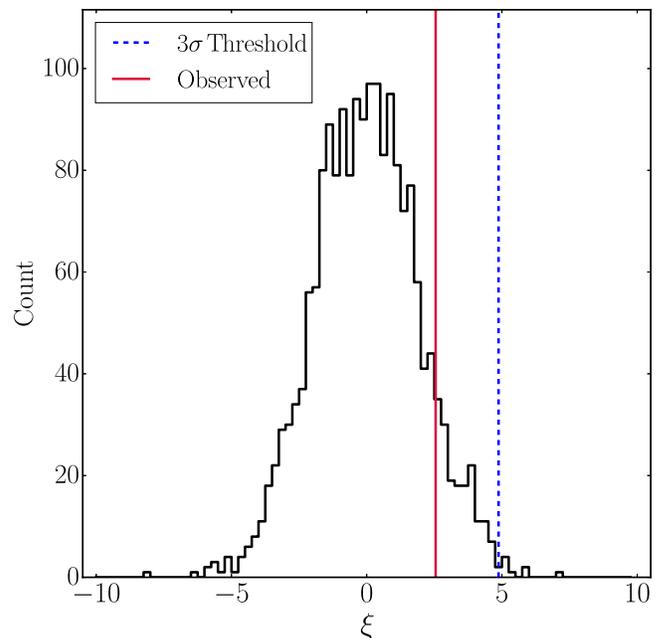
Figure 5. The distribution of the significances along with the threshold (dashed line) and the observed significance (red line) for the most significant FRB in this search. The significance is compared to the 3σ threshold obtained from the off-time period before and after each FRB.

7118 MeV^3. To find the upper limit on the neutrino flux at MeV energies, we evaluate the required time-integrated flux of antielectron neutrinos that would produce an enhancement in the signal rate in the detector corresponding to a 90% one-sided confidence level for the Gaussian distribution of the significance in the off-time runs. The 90% one-sided confidence level for a Gaussian in ξ is given by

$$\xi^{90} = \xi_{\text{th}} + z_{90} \cdot \sigma_\xi, \tag{6}$$
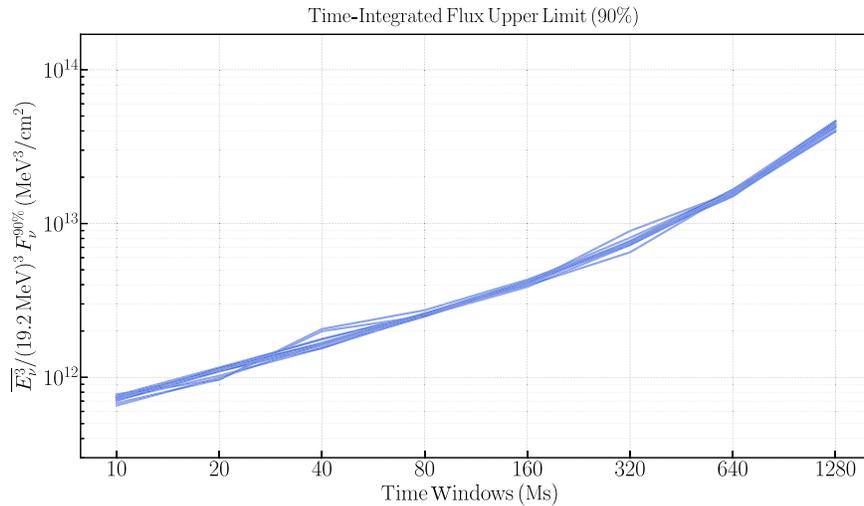
Figure 6. The 90% C.L. on the time-integrated flux of antielectron neutrinos from 21 FRBs considered in the analysis, assuming the fiducial model for neutrino emission with a mean neutrino energy of 15.6 MeV.

where ξ_{th} is the significance threshold, σ_ξ is the width of the significance distribution, and $z_{90} \approx 1.282$ is the fraction of the Gaussian width (1σ) representing the 90% confidence level interval. The significance for which one finds $\xi < \xi_{cut}$ only in 10% of random draws is denoted by ξ^{90}. The corresponding additional hits per DOM will be

$$\Delta\mu^{90} = \sigma_{\Delta\mu}(\xi_{th} + z_{90} \cdot \sigma_\xi). \quad (7)$$

The total increase in the signal hit rates in the detector is obtained by adding the signal of all DOMs. The upper limit on the time-integrated flux for FRBs considered in this analysis is shown in Figure 6.

4. Conclusion and Discussion

In two searches for neutrino emission from FRBs—one for tracklike events from muon neutrinos above 100 GeV and the other for MeV neutrino events—no significant association has been found.

We set upper limits (90% confidence level) on the time-integrated neutrino flux from FRBs that are the most constraining to date. For a power-law spectrum E^{-2} (E^{-3}), the limit set for GeV–TeV neutrinos is $E^2F < 2 \times 10^{-3}$ GeV cm^{-2} ($E^2F < 2 \times 10^{-4}$ GeV cm^{-2} at 100 TeV) per burst for emission timescales less than 10 s. We also set the first upper limits on MeV neutrino emission from FRBs: $\langle E^3 \rangle F < 8 \times 10^{11}$ MeV^3 cm^{-2} at an emission timescale of 10 ms (Figure 6).

In the tracks search, IceCube is more sensitive in the northern sky than in the southern sky, where most FRB sources have been detected so far. In addition, the stacking sensitivity scales with roughly the number of sources for which detection of a spatially coincident background event is unlikely within the time window. Therefore, as more FRBs are detected, especially in the northern sky by observatories like the Canadian Hydrogen Intensity Mapping Experiment (CHIME; Amiri et al. 2018, 2019), the stacking analysis sensitivity can improve by orders of magnitude. With fields of view significantly larger than those of single-dish telescopes, new radio interferometers may detect several FRBs per day in the coming years (Newburgh et al. 2016; Amiri et al. 2018), accelerating this improvement.

The MeV neutrino search was made possible by the ability of IceCube to identify a burst of MeV neutrinos on top of the background noise in the detector. While this capability has been primarily incorporated for obtaining early alerts on supernova explosions, it offers a unique opportunity for temporal study of low-energy neutrino -emission from transients. With this opportunity, we have placed the first-ever limits on neutrino signals at MeV energies from FRBs. Prospects for observation of an excess of MeV neutrinos in IceCube depends on the distance to the source. While IceCube is highly sensitive for identification of MeV signals from Galactic distances, there is growing evidence that most FRBs are extragalactic now that the redshift has been measured for two sources (Bannister et al. 2019; Ravi et al. 2019). It is worth mentioning that, in addition, on request, all untriggered DOM hits in the detector may be stored for any particular time period for several days (Aartsen et al. 2017). IceCube has used this channel to search for neutrino emission from gravitational wave sources. For more details, see Abbasi et al. (2017).

ORCID iDs

M. Ahlers ⓘ https://orcid.org/0000-0003-0709-5631
E. Bernardini ⓘ https://orcid.org/0000-0003-3108-1141
P. Dave ⓘ https://orcid.org/0000-0002-3879-5115
J. J. DeLaunay ⓘ https://orcid.org/0000-0001-5229-1995
P. A. Evenson ⓘ https://orcid.org/0000-0001-7929-810X
A. Franckowiak ⓘ https://orcid.org/0000-0002-5605-2219
U. Katz ⓘ https://orcid.org/0000-0002-7063-4418
A. Kheirandish ⓘ https://orcid.org/0000-0001-7074-0539
H. Pandya ⓘ https://orcid.org/0000-0002-6138-4808
A. Pizzuto ⓘ https://orcid.org/0000-0002-8466-8168
M. Santander ⓘ https://orcid.org/0000-0001-7297-8217
J. Vandenbroucke ⓘ https://orcid.org/0000-0002-9867-6548

References

Aartsen, M., Ackermann, M., Adams, J., et al. 2018c, Sci, 361, eaat1378
Aartsen, M. G., Abraham, K., Ackermann, M., et al. 2015a, ApJ, 809, 98
Aartsen, M. G., Abraham, K., Ackermann, M., et al. 2015b, PhRvL, 115, 081102
Aartsen, M. G., Ackermann, M., Adams, J., et al. 2017, JInst, 12, P03012
Aartsen, M. G., Ackermann, M., Adams, J., et al. 2018a, ApJ, 857, 117
Aartsen, M. G., Ackermann, M., Adams, J., et al. 2018b, Sci, 361, 147
Aartsen, M. G., Ackermann, M., Adams, J., et al. 2019, PhRvL, 122, 051102
Abbasi, R., Abdou, Y., Abu-Zayyad, T., et al. 2011, A&A, 535, A109
Abbasi, R., Andre, M., Anghinolfi, M., et al. 2017, PhRvD, 96, 022005
Albert, A., Andre, M., Anghinolfi, M., et al. 2017, PhRvD, 96, 082001
Albert, A., Andre, M., Anghinolfi, M., et al. 2019, MNRAS, 482, 184
Amiri, M., Bandura, K., Berger, P., et al. 2018, ApJ, 863, 48
Amiri, M., Bandura, K., Bhardwaj, M., et al. 2019, Natur, 566, 230
Bannister, K. W., Deller, A. T., Phillips, C., et al. 2019, Sci, 365, 565
Baum, V., Eberhardt, B., Fritz, A., Heereman, D., & Riedel, B. 2015, ICRC (The Hague), 34, 1096
Bhandari, S., Keane, E. F., Barr, E. D., et al. 2018, MNRAS, 475, 1427
Callister, T., Kanner, J., & Weinstein, A. 2016, ApJL, 825, L12
Das Gupta, P., & Saini, N. 2017, JApA, 39, 14
Desiati, P. 2011, Proc. ICRC (Beijing), 32, 78
Fahey, S., Kheirandish, A., Vandenbroucke, J., & Xu, D. 2017, ApJ, 845, 14
Grashorn, E. W., de Jong, J. K., Goodman, M. C., et al. 2010, APh, 33, 140
Haack, C., & Weibush, C. 2017, ICRC (Busan), 35, 1005
Keane, E. F. 2018, arXiv:1811.00899
Li, X., Zhou, B., He, H.-N., Fan, Y.-Z., & Wei, D.-M. 2014, ApJ, 797, 33
Lorimer, D. R. 2018, arXiv:1811.00195
Newburgh, L. B., Bandura, K., Bucher, M. A., et al. 2016, Proc. SPIE, 9906, 99065X
Petroff, E., Barr, E. D., Jameson, A., et al. 2016, PASA, 33, e045
Platts, E., Weltman, A., Walters, A., et al. 2018, arXiv:1810.05836
Ravi, V., Catha, M., Addario, L. D., et al. 2019, Natur, 572, 352
Tilav, S., Desiati, P., Kuwabara, T., et al. 2010, arXiv:1001.0776
Totani, T., Sato, K., Dalhed, H. E., & Wilson, J. R. 1998, ApJ, 496, 216